ARTICLES
https://doi.org/10.1038/s41594-018-0151-4

nature structural & molecular biology

High-resolution crystal structure of parathyroid hormone 1 receptor in complex with a peptide agonist

Janosch Ehrenmann[1,4], Jendrik Schöppe[1,4], Christoph Klenk[1,4*], Mathieu Rappas[2], Lutz Kummer[1,3], Andrew S. Doré[2] and Andreas Plückthun[1*]

Parathyroid hormone 1 receptor (PTH1R) is a class B multidomain G-protein-coupled receptor (GPCR) that controls calcium homeostasis. Two endogenous peptide ligands, parathyroid hormone (PTH) and parathyroid hormone–related protein (PTHrP), activate the receptor, and their analogs teriparatide and abaloparatide are used in the clinic to increase bone formation as an effective yet costly treatment for osteoporosis. Activation of PTH1R involves binding of the peptide ligand to the receptor extracellular domain (ECD) and transmembrane domain (TMD), a hallmark of class B GPCRs. Here, we present the crystal structure of human PTH1R in complex with a peptide agonist at 2.5-Å resolution, allowing us to delineate the agonist binding mode for this receptor and revealing molecular details within conserved structural motifs that are critical for class B receptor function. Thus, this study provides structural insight into the function of PTH1R and extends our understanding of this therapeutically important class of GPCRs.

PTH and the closely related PTHrP are critical regulators of mineral ion homeostasis, skeletal development and bone metabolism[1]. Both hormones mediate their effects through binding to PTH1R, which is primarily expressed in the kidney and bone.

When secreted from the parathyroid glands, PTH increases blood calcium levels by triggering reabsorption of calcium in the kidney and release of calcium from the bone. However, intermittently administered PTH was found to increase bone formation and mineralization[2]. These opposing effects are both mediated through activation of PTH1R, making this receptor a key target for the treatment of osteoporosis and severe dysregulation of calcium homeostasis[3]. Recently, teriparatide and abaloparatide, analogs of PTH and PTHrP, respectively, have been approved for use in the clinic to increase bone formation and mineralization, representing one of the most effective treatments available for osteoporosis[4,5]. Nonetheless, this treatment is costly and requires daily injections.

Despite immense efforts to design and develop potent PTH1R agonists, there are no efficient orally available drugs for the treatment of osteoporosis to date, in part due to the lack of detailed structural information on PTH1R–ligand interactions. Therefore, to gain insight into the molecular mechanism of ligand binding at PTH1R, we have determined the high-resolution crystal structure of a PTH1R–agonist complex.

Results

Engineering of a stabilized receptor–peptide complex. To enable crystallization, the TMD of PTH1R was engineered toward higher expression yields and enhanced thermostability through employing a combined approach of directed evolution in yeast and alanine scanning mutagenesis (Supplementary Fig. 1). The modified TMD was then rejoined with the ECD for crystallization trials (details in Methods). However, initial crystallization attempts of PTH1R in complex with endogenous agonists did not yield crystals in lipidic cubic phase. Therefore, we engineered a PTH mimetic agonist, termed ePTH, which strongly stabilized the receptor at only slightly reduced affinity and potency compared with wild-type (wt) PTH (residues 1–34) (Supplementary Fig. 2). These combined efforts of protein and peptide engineering allowed us to determine the structure of PTH1R at a resolution of 2.50 Å (Fig. 1a, Table 1, and Supplementary Figs. 3 and 4).

Overall architecture of the PTH1R structure. Globally, the PTH1R–ePTH structure displays the hallmarks of full-length class B GPCRs, with the ePTH peptide ligand connecting the ECD to the TMD of the receptor, burying a total surface area of 2,063 Å^2, and thus providing further evidence for the two-domain peptide ligand-binding model proposed for this receptor family (Fig. 1a). The overall conformation of the PTH1R ECD is similar to that previously reported for the isolated ECD[6], with the three-layer α-β-β-α fold forming the central hydrophobic groove for ligand interaction (PDB 3C4M, main chain atoms r.m.s. deviation = 0.64 Å) (Supplementary Fig. 5a). The TMD exhibits the canonical bundle of seven transmembrane helices (I–VII), with the orthosteric peptide-binding cavity adopting a V-shaped open conformation characteristic of class B GPCRs. Careful comparisons with other active and inactive class B GPCR–peptide ligand complexes suggest that the TMD of PTH1R is captured in a transitional state toward activation at the extracellular portion of the receptor, but the cytosolic half of the TMD remains in an inactive conformation.

PTH1R binding mode of ePTH. Within the ECD, ePTH residues 20–34 are bound as an amphipathic α-helix using W_{23}, L_{24}, K_{27}, L_{28}, V_{31} and Y_{34} (subscript indicates ePTH residue number) to interact with the hydrophobic surface (Fig. 2b; ePTH–PTH1R interactions

[1]Department of Biochemistry, University of Zürich, Zurich, Switzerland. [2]Sosei Heptares, Granta Park, Cambridge, UK. [3]Present address: Heptares Therapeutics Zürich AG, Schlieren, Switzerland. [4]These authors contributed equally: Janosch Ehrenmann, Jendrik Schöppe and Christoph Klenk.
*e-mail: c.klenk@bioc.uzh.ch; plueckthun@bioc.uzh.ch

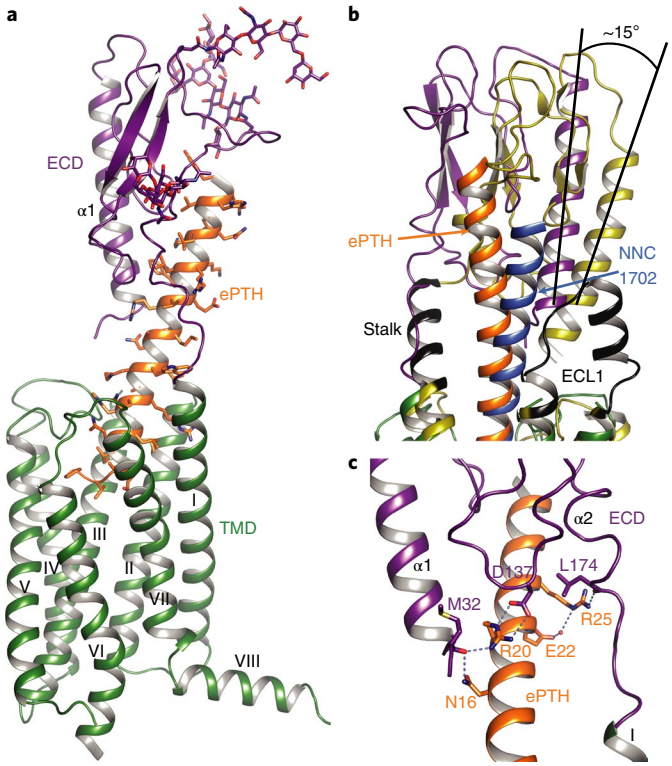

Fig. 1 | PTH1R–ePTH complex crystal structure. a, Overview of the PTH1R–ePTH complex structure, viewed from the membrane plane (TMD depicted in green, ECD in purple and ePTH in orange). Structurally resolved glycosylations of the ECD and ePTH side chains are shown in stick representation, with oxygen and nitrogen atoms in red and blue, respectively. **b**, Superposition of the extracellular parts of PTH1R–ePTH (color scheme same as in **a**) and GCGR–NNC1702 (yellow and blue, PDB 5YQZ) complexes. Secondary structural elements of the stalk and ECL1 only present in the GCGR structure are highlighted in black. The difference in ECD orientation relative to the aligned TMDs is indicated by an axis drawn through helix α1 of each ECD. **c**, Molecular details of specific interactions between ePTH and the juxtamembrane part of the ECD. with hydrogen bonds indicated by dashed blue lines. An ordered water molecule coordinated between E22 and R25 is shown as a red sphere.

Table 1 | Data collection and refinement statistics

	PTH1R–ePTH (PDB 6FJ3)
Data collection	
Space group	*P*1
Cell dimensions	
a, *b*, *c* (Å)	44.12, 52.86, 111.87
α, *β*, *γ* (°)	80.63, 83.76, 79.16
Resolution (Å)	49.39–2.50 (2.50–2.60)[a]
R_{merge}[c], R_{pim}[d]	0.153 (1.662), 0.103 (1.214)
$I/\sigma(I)$	5.2 (0.9)
$CC_{1/2}$	0.994 (0.501)
Completeness (%)	99.8 (99.3)
Redundancy	5.3 (4.7)
Refinement	
Resolution (Å)	49.39–2.50
No. reflections	33,646 (1,658)
R_{work} / R_{free}[e]	0.207 / 0.251
No. atoms	5,351
Protein	3,009
Fusion	1,536
Ligand	302
Waters, glycans, lipids	504
B factors	81.52
Protein	92.10
Fusion	51.66
Ligand	86.67
Waters, glycans, lipids	91.70
R.m.s. deviations	
Bond lengths (Å)	0.001
Bond angles (°)	0.484

X-ray diffraction data from 12 PTH1R–ePTH crystals were used to solve the structure. [a]Values in parentheses are for highest-resolution shell. [b]$R_{merge} = \Sigma_{hkl} \Sigma_i |I_i - \langle I \rangle| / - \Sigma_{hkl} \Sigma I_i$, where I_i is the intensity of the ith observation, <I> is the mean intensity of the reflection, and the summations extend over all unique reflections (hkl) and all equivalents (i), respectively. [c]$R_{pim} = \Sigma_{hkl} [n/(n-1)]^{1/2} \Sigma_i |I_i(hkl) - \langle I(hkl) \rangle| / \Sigma_{hkl} \Sigma_i I_i(hkl)$, where n is the multiplicity and all other variables are as defined for R_{merge}. [d]$R_{work} = \Sigma_{hkl} |F_o - F_c| / \Sigma_{hkl} F_o$, where F_o and F_c are observed and calculated structure factors, respectively. $R_{free} = \Sigma_T |F_o - F_c| / \Sigma_T F_o$, where T is a test dataset of about 5% of the total reflections randomly chosen and excluded from refinement.

listed in Supplementary Table 1; electron density map of interacting residues shown in Supplementary Fig. 4). ePTH adopts the same interactions described for wt PTH bound to the isolated ECD[6], with the exception of Nle_{18} (M_{18} in wt PTH), which faces away from the ECD and is not involved in binding, and Y_{34} (F_{34} in wt PTH), which is buried below a fucose moiety of a glycan resolved at N161. However, in line with previous studies on PTH1R[6,7], no effect of receptor glycosylation on ligand binding was observed (Supplementary Fig. 5d,e), in contrast with recent findings for the calcitonin receptor[8,9]. The peptide agonist maintains a helical conformation across the region that bridges the ECD and TMD (Fig. 1a), and the binding pose and orientation of ePTH in PTH1R are similar to those for other class B peptide agonists[10–12]. However, the PTH1R–ePTH complex does not exhibit secondary structural elements previously defined as the stalk of the glucagon receptor (GCGR)[12–14]. More in line with the GLP1 receptor (GLP1R), where this particular region has not been resolved, the PTH1R crystal structure has relatively high *B* factors within this short stretch of amino acids (T175–R179), suggesting a higher degree of conformational flexibility[10,11,14–16] (Fig. 1b and Supplementary Fig. 3g).

Previous structures of GLP1R and GCGR have indicated that the ligand-bound ECD is stabilized by interactions with extracellular loop 1 (ECL1)[10–12,17], which, for GCGR, has been shown to be crucial for receptor activation[14,16]. In contrast, the exceptionally long ECL1 of PTH1R is not resolved in the structure, suggesting that the relative orientation between the ECD and the TMD of PTH1R is primarily defined by the peptide agonist itself. In line with this observation, it was shown that ECL1 is not required for binding and activation of PTH1R[18–20]. Instead, the structure of PTH1R reveals an extended network of interactions formed between the ligand and the juxtamembrane part of the ECD. ePTH specifically interacts with the N- and C-terminal ends of helices α1 and α2, respectively, and the loop connecting β3 and β4 within the ECD. The backbone carbonyl of M32 makes a bifurcated hydrogen bond with both N_{16} and R_{20}. The latter residue is held in position by an ionic interaction with D137 of the ECD across an extended electronic network spanning 10 Å, and this interaction is essential for ligand binding and receptor activation[21]. The side chain of R_{25} is poised to hydrogen-bond via a water molecule to the side chain of E_{22} and to the main chain carbonyl of L174 at the junction of the ECD α1 helix and the linker region of the receptor (Fig. 1c). ePTH is in a conformation similar to that of the crystal structure of isolated wt PTH (PDB 1ET1; r.m.s. deviation

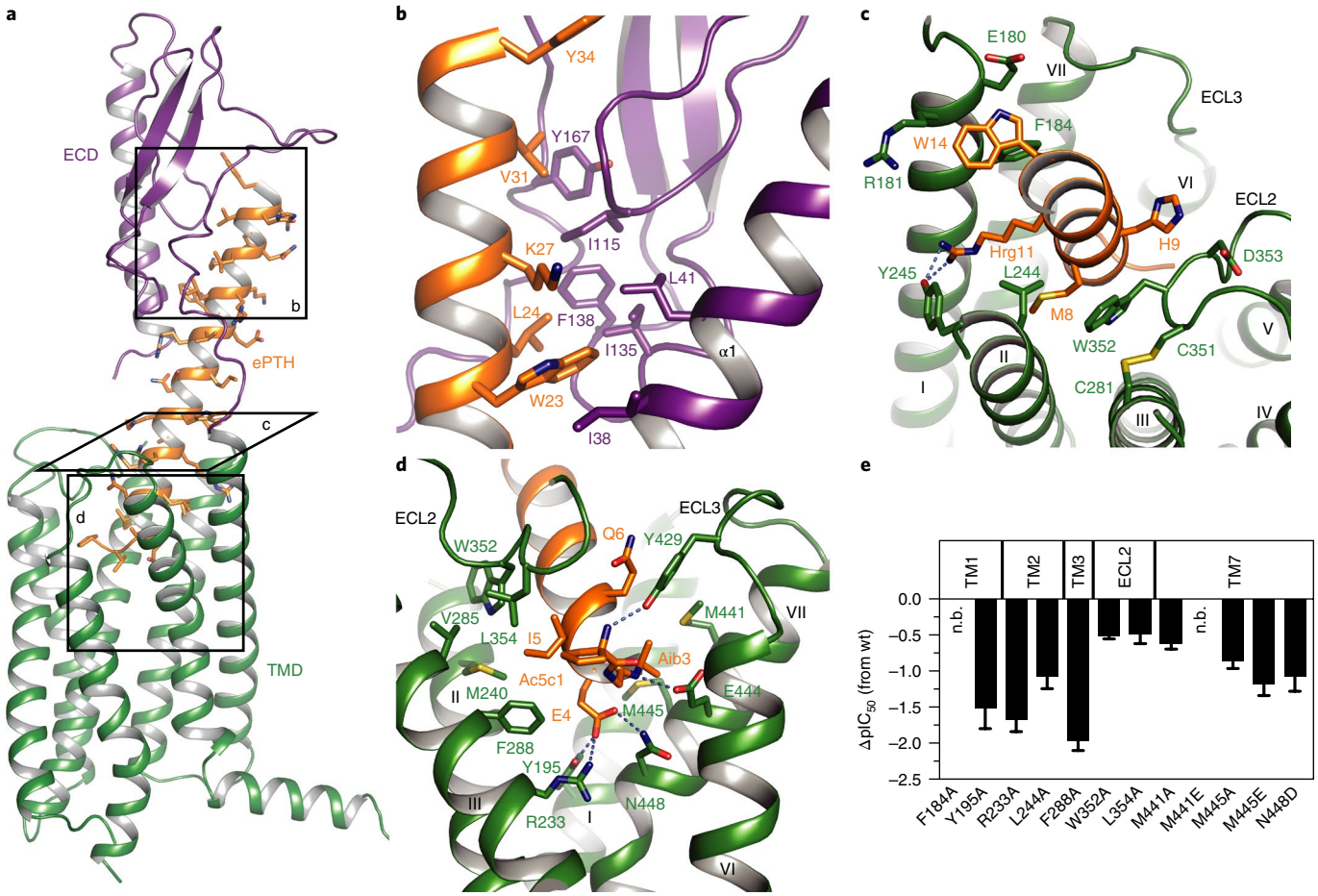

Fig. 2 | Structural and functional details of PTH1R–ePTH interactions. a, Overview of the PTH1R–ePTH complex structure. Black boxes indicate positions of close-up views shown in **b**–**d**. **b**, Close-up of specific interactions between ePTH and the ECD of PTH1R. **c**,**d**, Close-ups of specific ePTH interactions within the orthosteric binding pocket of the PTH1R TMD. **e**, Ligand affinity profiles of selected mutants (wt PTH1R background) in comparison with wt PTH1R. IC_{50} values were derived from whole-cell ligand competition-binding experiments with wt PTH(1–34) (Supplementary Fig. 7 and Supplementary Table 2). Bars represent the mean change ± s.e.m. in calculated affinity (ΔpIC_{50}) for each mutant compared with wt receptor. Numbers of independent experiments performed in duplicate are listed in Supplementary Table 2. n.b., no binding.

= 1.02 Å), exhibiting a slight bend between residues 12–21 (ref. [22]) (Supplementary Fig. 5b,c). Interestingly, this conformation of the peptide requires a tilt of the ECD by ~15° toward helix VII, in comparison with the GCGR structure (Fig. 1b), which may be crucial for receptor function, because the mid-region conformation of PTH peptides has been shown to influence ligand potency[23,24]. Therefore, the PTH1R–ePTH complex structure reveals a potential additional mode of class B GPCR complex stabilization in the absence of specific contacts that wedge and position the peptide ligand in the more flexible region connecting the ECD to the TMD. At least for PTH1R, the orientation of the two domains is thus mediated by the peptide ligand helical propensity and rigidity rather than by additional stabilizing interactions.

Within the orthosteric binding pocket of the TMD, residues 1–14 of ePTH run parallel to helix II, making contacts with residues in helices I, II, III, VII and ECL2 and ECL3 (Fig. 2c). The extracellular boundary of the pocket is defined by W_{14}, making hydrophobic interactions with $F184^{1.36}$ (superscript indicates Wootten numbering scheme for class B GPCRs[25]) and the aliphatic portion of $E180^{1.32}$ and $R181^{1.33}$ at the extracellular tip of helix I. The ligand is stacked against helices II, III and ECL2, with its orientation locked by the homoarginine (Hrg) at position 11, intercalating between helix I and II, similar to Y_{10} of the glucagon analog NNC1702 and the X2 moiety of the engineered GLP1R agonist peptide 5 (refs. [12,17]). Hrg_{11} occupies a hydrophobic cleft lined by residues $F184^{1.36}$ and $L244^{2.71}$, with the polar head group hydrogen-bonding to the hydroxyl group of $Y245^{2.72}$. The extended hydrophobic interaction between the aliphatic portion of Hrg_{11}, $F184^{1.36}$ and $L244^{2.71}$ provides a structural rationale for the enhanced potency of L_{11} substitutions in wt PTH, with amino acids more complementary to this local environment[26]. One helical turn further into the binding pocket, the aliphatic portion of Q_6 is found stacked against $Y429^{ECL3}$, with L_7 and M_8 making hydrophobic interactions with helices I and II (Fig. 2d). $W352^{ECL2}$ wedges between the peptide main chain atoms, linking M_8 and H_9 and the conserved extracellular receptor disulfide bridge formed between $C281^{3.29}$ and $C351^{ECL2}$ with the side chain of H_9 further stacked against the aliphatic portion of $D353^{ECL2}$ (Fig. 2c). Interestingly, in all other structures of peptide-bound class B GPCRs, this conserved tryptophan in ECL2 is positioned between transmembrane helices III and IV (Supplementary Fig. 6a,b). ECL2 further interacts with I_5 of ePTH, which is located in a hydrophobic subpocket lined by $M240^{2.67}$, $V285^{3.33}$, $W352^{ECL2}$ and $L354^{ECL2}$ and stacked against $F288^{3.36}$. I_5 has previously been shown to be a key peptide residue determinant for inducing a G-protein-independent high-affinity conformation of PTH1R[27,28], and, consequently, mutation of $F288^{3.36}$ to alanine severely reduces ligand binding affinity (Fig. 2d,e).

Toward the bottom of the binding pocket, the N-terminal 1-aminocyclopentane-1-carboxylic acid ($Ac5c_1$) and V_2 of ePTH adopt a nonhelical conformation (N-cap), in agreement with

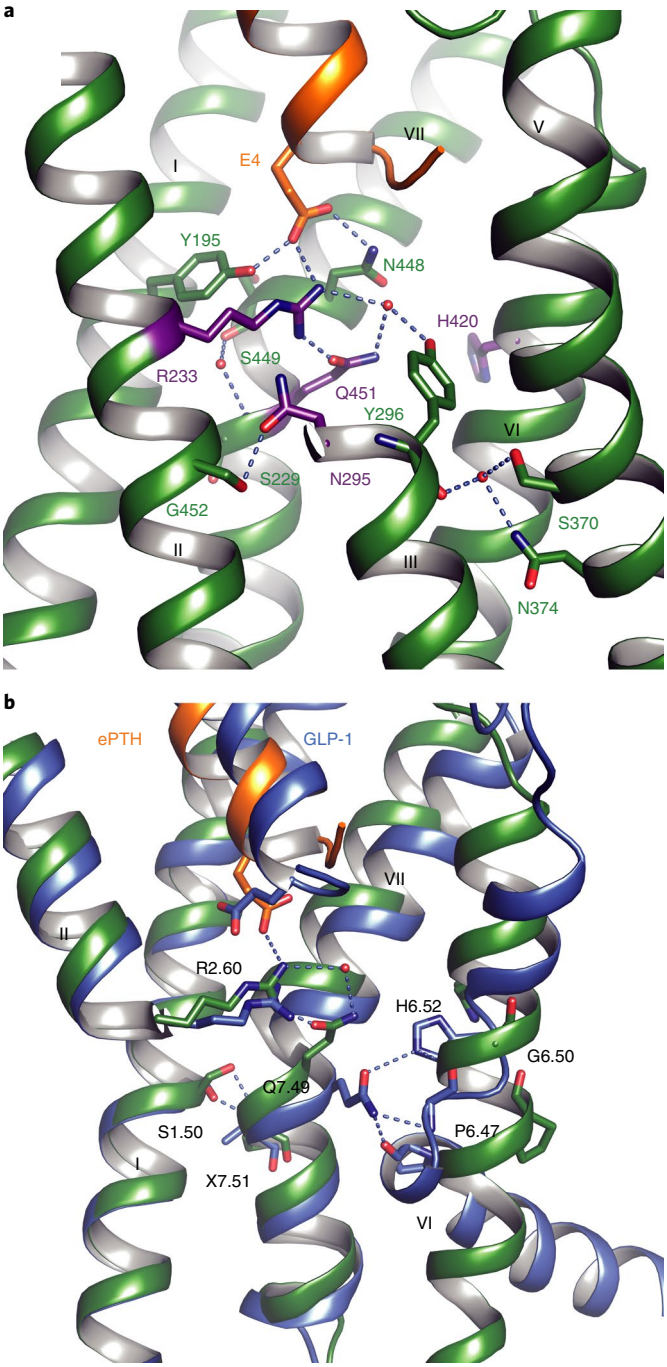

Fig. 3 | Water-mediated extension and conformational changes upon activation in the central polar network. a, Central polar network at the base of the orthosteric pocket viewed from the membrane plane. Residues of the central polar network of class B GPCRs are highlighted as purple sticks; residues identified to further extend and stabilize the conformation of this network are depicted as green sticks. Ordered water molecules are shown as red spheres. **b**, Superposition of PTH1R and the G-protein-bound GLP1R–GLP1 complex (blue, PDB 5VAI). Conserved residues involved in ligand recognition and receptor activation are shown as sticks and labeled according to the Wootten scheme[25].

ligands in similar class B receptor structures[10,11,17,29,30]. The N-cap is positioned in proximity to helices V and VI, with $Ac5c_1$ pointing toward helix V and V_2 facing toward the lower extremity of the orthosteric pocket. The N terminus of PTH is implicated in receptor activation[31–33], and in our structure, the N-cap is poised to hydrogen-bond to the hydroxyl of $Y429^{ECL3}$. The position of the peptide N terminus is stabilized by a hydrogen bond between the peptide backbone nitrogen of α-aminoisobutyric acid at position 3 (Aib_3) and $E444^{7.42}$ of the receptor and, further, by the localization of the geminal dimethyl group of Aib_3 in a hydrophobic cleft between $M441^{7.39}$ and $M445^{7.43}$ (Fig. 2d). This subset of observed interactions between Aib_3, $M441^{7.39}$, $E444^{7.42}$ and $M445^{7.43}$ rationalizes the proposed critical role of the extracellular portion of helix VII for PTH affinity and potency[19,34], which is further underlined by the significant loss of peptide agonist affinity upon mutation of these residues (Fig. 2e and Supplementary Fig. 7). At the base of the ligand binding pocket, the side chain of E_4 of the ligand is pointing toward helices I and VII and hydrogen-bonding to $N448^{7.46}$, as well as to the highly conserved $Y195^{1.47}$ and $R233^{2.60}$; likewise, mutation of either of these residues to alanine results in strongly impaired ligand binding (Fig. 2d,e).

Central polar network. At the base of the orthosteric binding pocket $R233^{2.60}$, $N295^{3.43}$, $H420^{6.52}$ and $Q451^{7.49}$ form the previously defined central polar network (Fig. 3a), which is critically involved in receptor activation[9,11]. The high resolution of the PTH1R structure reveals several ordered waters within this network and thus allows us to further delineate important water-mediated extensions involving residues that are highly conserved across class B GPCRs (Supplementary Fig. 6g). E_4 of the agonist interacts with $R233^{2.60}$ (as previously suggested for GLP1R and GCGR), which is in direct contact with $Q451^{7.49}$ via a hydrogen bond, thereby relaying peptide recognition deeper into the receptor core. A water molecule establishes a central connection between helices II, III and VII by interacting with residues $R233^{2.60}$, $Y296^{3.44}$ and $Q451^{7.49}$ on the respective helices, providing a structural rationale for the critical role of $R233^{2.60}$ and $Q451^{7.49}$ for receptor activation[35]. The interaction of $S229^{2.56}$ with $N295^{3.43}$ and, furthermore, the water-mediated interaction of the backbone oxygen of $Y296^{3.44}$ with $S370^{5.46}$ and the conserved $N374^{5.50}$, stabilize the conformation of the interface between helices II, III, IV and V, which remains rigid during receptor activation.

Comparison of agonist-bound PTH1R with agonist- and G-protein-bound GLP1R[11] reveals several rearrangements within the central polar network upon receptor activation (Fig. 3b): the ligand-$R^{2.60}$-$Q^{7.49}$ relay is broken due to a downward movement of $Q^{7.49}$ toward helix VI. This reorientation allows $Q^{7.49}$ to stabilize the pronounced kink in helix VI caused by the outward movement of helix VI via hydrogen-bonding to the backbone oxygens of both $P^{6.47}$ and $G^{6.50}$ within the conserved $P^{6.47}$-x-x-$G^{6.50}$ motif. Furthermore, during activation, $H^{6.52}$ swings in between helices VI and VII and thus contributes to the stabilization of the kink of helix VI via interaction with $Q^{7.49}$ and the backbone oxygen of $G^{6.50}$. Interestingly, the stabilizing mutation $I458^{7.56}$A is facing toward $S409^{6.41}$ two helical turns below $G^{6.50}$. While small residues at this position would likely support the inactive conformation of helix VI, a sporadically occurring mutation to arginine leads to constitutive receptor activation, which is one of the causes for Jansen's Metaphyseal Chondrodysplasia associated with short limb dwarfism and hypercalcemia[36]. The proximity of both residues suggests that $R458^{7.56}$ could destabilize the intracellular part of helix VI and thus promote spontaneous receptor activation (Supplementary Fig. 8). Helix VII is also linked to helix I by the previously described hydrogen bond formed between the conserved $S^{1.50}$ and the backbone nitrogen of residues at position 7.51, located at the kink in helix VII (ref. [11]). This kink is further stabilized by a water molecule coordinated between $S^{7.47}$ and $G^{7.50}$.

Consequences of stabilizing mutations on receptor activation. Although the TMD of the PTH1R–ePTH complex is in an inactive conformation at the cytoplasmic side, the structure displays features

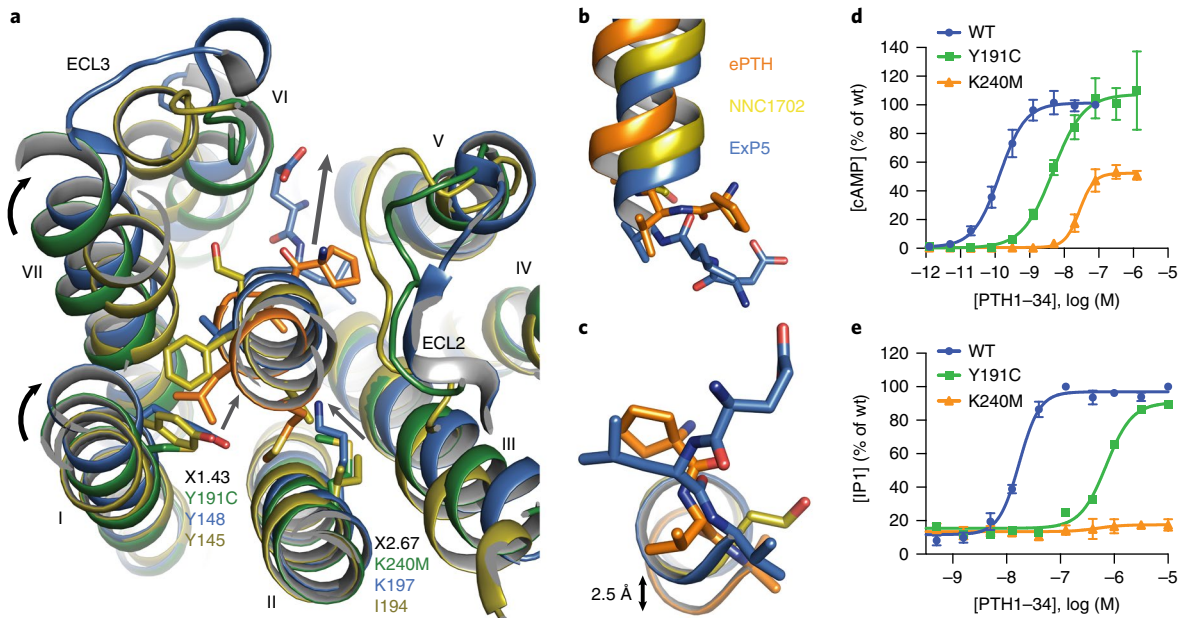

Fig. 4 | Influence of bulky residues in helices I and II on the activation of class B GPCRs. a, Extracellular view on superposed PTH1R–ePTH (color scheme same as in Fig. 1), GCGR–NNC1702 (yellow) and GLP1R–ExP5 (blue, PDB 6B3J) complexes. Conserved bulky residues (highlighted as sticks) at positions 1.43 and 2.67 of class B GPCRs lead to a push of the peptide ligand toward the interface between helices V and VI (indicated by gray arrows). The proposed movements of helices I and VII upon receptor activation are indicated by curved black arrows. **b**,**c**, Superposition of peptide ligand N termini in side view (**b**) or intracellular view (**c**). **d**,**e**, Normalized concentration–response curves for cAMP (**d**) or IP1 (**e**) accumulation measured in HEK293T cells expressing wt or mutant PTH1R. Data are shown as mean values ± s.e.m. from five (**d**) or three (**e**) independent experiments performed in duplicates.

of an active-like conformation at the extracellular side. Helices I and VII are rotated clockwise along the central axis of the receptor, adopting an intermediate state when compared with the fully active GLP1R–ExP5–Gs complex and the structure of GCGR bound to a weak partial agonist[10,12] (Fig. 4a). Helix VI likewise exhibits a clockwise motion, but it remains in a position closer to the receptor core, in contrast with the widening of the binding pocket mediated through outward shifts of helices VI and VII in the active-state structures of GLP1R. This finding might be explained by the additional hydrogen bond between helices VI and VII formed by the stabilizing mutation Q440$^{7.38}$R, thereby constraining the outward movement of helix VI and thus preventing full receptor activation[19] (Supplementary Fig. 6c–f). While the binding pose and orientation of ePTH in PTH1R are similar to those of GLP1–ExP5 entering the binding pocket along helix II in GLP1R, ePTH is shifted away from the central helix bundle axis toward helices II and I. This shift is sterically enabled by the stabilizing mutations Y191$^{1.43}$C and K240$^{2.67}$M, replacing two bulky residues at the lower part of the binding pocket and allowing L_7 and M_8 of ePTH to be accommodated into a cleft formed by helices I, II and VII (Fig. 4a–c). As a consequence, the N terminus of ePTH is shifted away from helices V and VI and thus may not be able to displace helix VI at the opposite side of the receptor into a signaling-active conformation. This observation may structurally explain the significantly impaired signaling activity conferred by each of the two mutations in the wt receptor background (Fig. 4d,e), similar to the inhibitory effect of N-terminal truncations on class B peptide agonists.

Discussion

PTH1R is a prototypical member of the class B family of GPCRs, which have in common that their ligands are long helical peptides contacting both the ECD and the TMD[37], and that ligand binding is believed to occur in a two-step mechanism[38]. Because the peptide ligands of class B receptors play central roles in the regulation of fundamental physiological processes, such as the metabolism of glucose and control of mineral ion homeostasis, class B GPCRs are, thus, important drug targets for a number of severe, chronic human diseases. Yet, for a long time, structural information was limited to the ECD alone (summarized in ref. [39]) before structures of the isolated TMD became available[13,40,41]. Only recently have the full-length structures of class B receptors become available, and detailed structural insight into peptide–receptor recognition has been elucidated for CTR[9], GLP1R[10,11,17] and GCGR[12]. These breakthroughs are important steps on the path toward the rational development of new drugs for indications such as diabetes and obesity.

With more than 200 million people affected, osteoporosis is one of the most prevalent diseases worldwide, and osteoporosis-related incidences are predicted to increase twofold in aging populations within the next 20 years[42]. Recombinant analogs of PTH and PTHrP are currently the most effective drugs for the treatment of severe osteoporosis, but as daily injectables with high costs, probably not suitable for treatment of such a widespread disease. The crystal structure of the human PTH1R in complex with a peptide agonist presented here provides, for the first time, detailed insight into the molecular architecture of this receptor, opening the opportunity to use this structure as a base for designing new chemical entities in the future.

The determination of the PTH1R structure has become possible only by extensive engineering of the receptor. Remarkably, the stabilizing effect of several mutations appears to be linked to interference with conserved networks that are critical for propagation of receptor activation through the transmembrane core. Furthermore, because native ligands of PTH1R did not yield crystals, it was necessary to use a modified PTH peptide agonist, which is similar to a previously described ligand reported to induce prolonged signaling responses on the PTH1R[27]. Therefore, it is tempting to speculate that such modified peptides that are able to act as agonists with the wt receptor also take on a similar orientation in the stabilized receptor, because the binding interactions, probed by mutations, are fully consistent between the wt and the stabilized receptors. The stabilized

receptor, however, no longer induces GDP–GTP exchange in the heterotrimeric G protein, and thus, the mutations that have been introduced in the necessary stabilization must interfere with the conformational change subsequent to agonist binding, allowing some conclusions to be made about the mechanism of this conformational change (last section of Results).

In PTH1R, our structure suggests that the relative orientation between the ECD and the TMD of PTH1R is primarily defined by the helical peptide agonist itself. This is in contrast with GCGR and GLP1R, in which the ligand-bound ECD appears to be stabilized by interactions with ECL1, and in the case of GCGR, ECL1 has been shown to be crucial for receptor activation[14,16]. ECL1 of PTH1R, in contrast, is exceptionally long and not resolved in the structure. This finding suggests that there are some differences between the class B receptors, and it will be necessary to determine the structures of further family members to assess whether there are additional modes of interactions in this family.

In conclusion, the crystal structure of the PTH1R–ePTH complex provides, for the first time, insight into the intricate details of peptide agonist recognition and binding at this physiologically important receptor, pointing out similarities and differences to other class B receptors, as far as their structures are currently known. The high resolution achieved here allows an exact description of conserved activation motifs, including ordered waters, and thus increases the general understanding of class B receptor activation. We anticipate that our findings will support and facilitate the development of novel therapeutics, not only for PTH1R but for all class B GPCRs as important therapeutic targets for a variety of diseases.

Online content

Any methods, additional references, Nature Research reporting summaries, source data, statements of data availability and associated accession codes are available at https://doi.org/10.1038/s41594-018-0151-4.

Received: 10 July 2018; Accepted: 8 October 2018;
Published online: 19 November 2018

References

1. Gardella, T. J. & Vilardaga, J.-P. International Union of Basic and Clinical Pharmacology. XCIII. The parathyroid hormone receptors–family B G protein-coupled receptors. *Pharmacol. Rev.* **67**, 310–337 (2015).
2. Selye, H. On the stimulation of new bone-formation with parathyroid extract and irradiated ergosterol. *Endocrinology* **16**, 547–558 (1932).
3. Cheloha, R. W., Gellman, S. H., Vilardaga, J.-P. & Gardella, T. J. PTH receptor-1 signalling-mechanistic insights and therapeutic prospects. *Nat. Rev. Endocrinol.* **11**, 712–724 (2015).
4. Miller, P. D. et al. Effect of abaloparatide vs placebo on new vertebral fractures in postmenopausal women with osteoporosis: a randomized clinical trial. *JAMA* **316**, 722–733 (2016).
5. Kendler, D. L. et al. Effects of teriparatide and risedronate on new fractures in post-menopausal women with severe osteoporosis (VERO): a multicentre, double-blind, double-dummy, randomised controlled trial. *Lancet* **391**, 230–240 (2017).
6. Pioszak, A. A. & Xu, H. E. Molecular recognition of parathyroid hormone by its G protein-coupled receptor. *Proc. Natl Acad. Sci. USA* **105**, 5034–5039 (2008).
7. Bisello, A. et al. Role of glycosylation in expression and function of the human parathyroid hormone/parathyroid hormone-related protein receptor. *Biochemistry* **35**, 15890–15895 (1996).
8. Lee, S.-M. et al. N-Glycosylation of asparagine 130 in the extracellular domain of the human calcitonin receptor significantly increases peptide hormone affinity. *Biochemistry* **56**, 3380–3393 (2017).
9. Liang, Y.-L. et al. Phase-plate cryo-EM structure of a class B GPCR-G-protein complex. *Nature* **546**, 118–123 (2017).
10. Liang, Y.-L. et al. Phase-plate cryo-EM structure of a biased agonist-bound human GLP-1 receptor–Gs complex. *Nature* **68**, 954 (2018).
11. Zhang, Y. et al. Cryo-EM structure of the activated GLP-1 receptor in complex with a G protein. *Nature* **546**, 248–253 (2017).
12. Zhang, H. et al. Structure of the glucagon receptor in complex with a glucagon analogue. *Nature* **553**, 106–110 (2018).
13. Siu, F. Y. et al. Structure of the human glucagon class B G-protein-coupled receptor. *Nature* **499**, 444–449 (2013).
14. Zhang, H. et al. Structure of the full-length glucagon class B G-protein-coupled receptor. *Nature* **546**, 259–264 (2017).
15. Koth, C. M. et al. Molecular basis for negative regulation of the glucagon receptor. *Proc. Natl Acad. Sci. USA* **109**, 14393–14398 (2012).
16. Yang, L. et al. Conformational states of the full-length glucagon receptor. *Nat. Commun.* **6**, 7859 (2015).
17. Jazayeri, A. et al. Crystal structure of the GLP-1 receptor bound to a peptide agonist. *Nature* **546**, 254–258 (2017).
18. Lee, C. et al. Role of the extracellular regions of the parathyroid hormone (PTH)/PTH-related peptide receptor in hormone binding. *Endocrinology* **135**, 1488–1495 (1994).
19. Lee, C. et al. Homolog-scanning mutagenesis of the parathyroid hormone (PTH) receptor reveals PTH-(1-34) binding determinants in the third extracellular loop. *Mol. Endocrinol.* **9**, 1269–1278 (1995).
20. Zhao, L.-H. et al. Differential requirement of the extracellular domain in activation of class B G protein-coupled receptors. *J. Biol. Chem.* **291**, 15119–15130 (2016).
21. Weaver, R. E., Wigglesworth, M. J. & Donnelly, D. A salt bridge between Arg-20 on parathyroid hormone (PTH) and Asp-137 on the PTH1 receptor is essential for full affinity. *Peptides* **61**, 83–87 (2014).
22. Jin, L. et al. Crystal structure of human parathyroid hormone 1-34 at 0.9-A resolution. *J. Biol. Chem.* **275**, 27238–27244 (2000).
23. Condon, S. M. et al. The bioactive conformation of human parathyroid hormone. structural evidence for the extended helix postulate. *J. Am. Chem. Soc.* **122**, 3007–3014 (2000).
24. Mierke, D. F. et al. Conformational studies of mono- and bicyclic parathyroid hormone-related protein-derived agonists. *Biochemistry* **36**, 10372–10383 (1997).
25. Wootten, D., Simms, J., Miller, L. J., Christopoulos, A. & Sexton, P. M. Polar transmembrane interactions drive formation of ligand-specific and signal pathway-biased family B G protein-coupled receptor conformations. *Proc. Natl Acad. Sci. USA* **110**, 5211–5216 (2013).
26. Shimizu, M., Carter, P. H., Khatri, A., Potts, J. T. & Gardella, T. J. Enhanced activity in parathyroid hormone-(1-14) and -(1-11): novel peptides for probing ligand-receptor interactions. *Endocrinology* **142**, 3068–3074 (2001).
27. Okazaki, M. et al. Prolonged signaling at the parathyroid hormone receptor by peptide ligands targeted to a specific receptor conformation. *Proc. Natl Acad. Sci. USA* **105**, 16525–16530 (2008).
28. Dean, T., Vilardaga, J.-P., Potts, J. T. & Gardella, T. J. Altered selectivity of parathyroid hormone (PTH) and PTH-related protein (PTHrP) for distinct conformations of the PTH/PTHrP receptor. *Mol. Endocrinol.* **22**, 156–166 (2008).
29. Inooka, H. et al. Conformation of a peptide ligand bound to its G-protein coupled receptor. *Nat. Struct. Biol.* **8**, 161–165 (2001).
30. Neumann, J.-M. et al. Class-B GPCR activation: is ligand helix-capping the key? *Trends. Biochem. Sci.* **33**, 314–319 (2008).
31. Tregear, G. W. et al. Bovine parathyroid hormone: minimum chain length of synthetic peptide required for biological activity. *Endocrinology* **93**, 1349–1353 (1973).
32. Goltzmann, D., Peytremann, A., Callahan, E., Tregear, G. W. & Potts, J. T. Analysis of the requirements for parathyroid hormone action in renal membranes with the use of inhibiting analogues. *J. Biol. Chem.* **250**, 3199–3203 (1975).
33. Rosenblatt, M. & Potts, J. T. Analogues of an in vitro parathyroid hormone inhibitor: modifications at the amino terminus. *Calcif. Tissue Int.* **33**, 153–157 (1981).
34. Gardella, T. J. et al. Determinants of [Arg2]PTH-(1-34) binding and signaling in the transmembrane region of the parathyroid hormone receptor. *Endocrinology* **135**, 1186–1194 (1994).
35. Gardella, T. J., Luck, M. D., Fan, M. H. & Lee, C. Transmembrane residues of the parathyroid hormone (PTH)/PTH-related peptide receptor that specifically affect binding and signaling by agonist ligands. *J. Biol. Chem.* **271**, 12820–12825 (1996).
36. Schipani, E. et al. A novel parathyroid hormone (PTH)/PTH-related peptide receptor mutation in Jansen's metaphyseal chondrodysplasia. *J. Clin. Endocrinol. Metab.* **84**, 3052–3057 (1999).
37. Hoare, S. R. J. Mechanisms of peptide and nonpeptide ligand binding to Class B G-protein-coupled receptors. *Drug Discov. Today* **10**, 417–427 (2005).
38. Castro, M., Nikolaev, V. O., Palm, D., Lohse, M. J. & Vilardaga, J.-P. Turn-on switch in parathyroid hormone receptor by a two-step parathyroid hormone binding mechanism. *Proc. Natl Acad. Sci. USA* **102**, 16084–16089 (2005).
39. Parthier, C., Reedtz-Runge, S., Rudolph, R. & Stubbs, M. T. Passing the baton in class B GPCRs: peptide hormone activation via helix induction? *Trends. Biochem. Sci.* **34**, 303–310 (2009).
40. Hollenstein, K. et al. Structure of class B GPCR corticotropin-releasing factor receptor 1. *Nature* **499**, 438–443 (2013).

41. Jazayeri, A. et al. Extra-helical binding site of a glucagon receptor antagonist. *Nature* **533**, 274–277 (2016).
42. Odén, A., McCloskey, E. V., Kanis, J. A., Harvey, N. C. & Johansson, H. Burden of high fracture probability worldwide: secular increases 2010-2040. *Osteoporos. Int.* **26**, 2243–2248 (2015).

Acknowledgements

We thank B. Blattmann of the Protein Crystallisation Center at the University of Zurich for his support with crystallization, the staff of the X06SA beamline at the Paul Scherrer Institute for support during data collection and I. Berger at the European Molecular Biology Laboratory for providing us with baculovirus transfer vectors. We also thank G. Meier and B. Aebli for support during protein production. This work was supported by Schweizerischer Nationalfonds Grants 31003A_153143 and 31003A_182334 and KTI grant 18022.1 PFLS-LS, all to A.P.; C.K. is the recipient of a fellowship of the German Academy of Sciences Leopoldina (LPDS 2009-48) and a Marie Curie fellowship of the European Commission (FP7-PEOPLE-2011-IEF #299208).

Author contributions

C.K., with the help of L.K., performed directed evolution in yeast. J.E. and J.S. carried out the rational mutagenesis for further thermostabilization of the receptor. J.E., J.S. and C.K. characterized expression constructs and optimized protein expression. J.E. and J.S. designed and characterized crystallization constructs; expressed, purified and crystallized PTH1R; and harvested crystals. J.E., J.S. and A.S.D. collected diffraction data. J.E., J.S., M.R. and A.S.D. processed the data and solved and refined the structure. C.K. performed pharmacological characterization. C.K. and A.P. designed the project. Project management was carried out by J.E., J.S., C.K. and A.P. The manuscript was prepared by J.E., J.S., C.K. and A.P. All authors contributed to the final editing and approval of the manuscript.

Competing interests

M.R., L.K. and A.S.D. are employees of Heptares Therapeutics, a company with activities in the GPCR field.

Additional information

Supplementary information is available for this paper at https://doi.org/10.1038/s41594-018-0151-4.

Reprints and permissions information is available at www.nature.com/reprints.

Correspondence and requests for materials should be addressed to C.K. or A.P.

Publisher's note: Springer Nature remains neutral with regard to jurisdictional claims in published maps and institutional affiliations.

Methods

Generation of well-expressing and thermostabilized PTH1R. To improve expression levels and stability of PTH1R, the predicted transmembrane region of the receptor (residues 178–480) was subjected to a directed evolution approach in *S. cerevisiae*, as previously described[43] using [Ac5c$_1$, Aib$_3$, Q$_{10}$, Hrg$_{11}$, A$_{12}$, W$_{14}$] PTH(1–14) (ref. [44]) that was labeled with HiLyte Fluor 647 at K$_{13}$ (Anaspec) as a ligand for FACS-based selections. In total, two randomization steps with 4 or 5 selection rounds each were conducted. The mutant PTH1R(Y191C K240M M312K V334I K359N Q440R) (denoted PTH1R-SaBRE), displaying the highest functional expression levels in *Spodoptera frugiperda* (*Sf*9) insect cells, was further thermostabilized in an agonist-bound state by substituting selected amino acids within the transmembrane helical bundle with either alanine or leucine (if the amino acid was an alanine) and evaluating the resulting mutants based on their gain in thermostability, as evidenced by an increase in T_m in the CPM assay[45]. Positions that displayed the highest gain in thermostability (L300A, L407A, A426L, I458A) were subsequently combined, yielding the stabilized transmembrane domain of PTH1R, termed PTH1R$_S$, used in this study (Supplementary Fig. 1b).

Cloning and expression of PTH1R crystallization construct. Prior to rejoining the ECD with the thermostabilized PTH1R$_S$ transmembrane domain, the ECD was modified as follows: the native signal peptide M1-Y23 and the unstructured residues S61–R104 (ref. [6]) were removed to prevent potential proteolytic cleavage[46]. The ECD (residues 24–177) was then joined with the transmembrane domain (residues 178–480), and in the same construct, the previously reported PGS domain[47] was fused into the third intracellular loop (ICL3) between residues K388 and D398. To further reduce flexibility for crystallization, the construct was C-terminally truncated at residue A480, yielding the final crystallization construct PTH1R$_{XTAL}$ (Supplementary Fig. 1a).

The gene was cloned into a modified pFL vector (MultiBac system, Geneva Biotech) resulting in a final expression construct with a melittin signal sequence followed by a FLAG-tag, His$_{10}$-tag and a human rhinovirus 3 C protease cleavage site N terminal to the receptor gene. For expression, *Sf*9 cells in Sf-900II SFM medium (Thermo Fisher Scientific) were infected with baculovirus at a density of 3×10^6 cells/ml, and expression was performed for 72 h at 27 °C under constant shaking.

Peptide design of ePTH. Because initial crystallization attempts employing commercially available native or modified PTH peptide ligands failed, ePTH was designed to improve the stability of the PTH1R–peptide complex. ePTH constitutes a chimera of the N-terminal 14 amino acid PTH mimetic optimized for high binding affinity at the isolated transmembrane domain[44] and the native 20 amino acid PTH peptide C terminus. Within this C terminus, two additional mutations, M$_{18}$Nle and F$_{34}$Y, including a C-terminal amide were introduced, which had been previously reported to increase stability and potency[6,48,49]. This modified peptide had only slightly reduced affinity and was found to be a partial agonist.

Purification of PTH1R–ePTH complex. Insect cells expressing PTH1R$_{XTAL}$ were lysed, and receptor-containing membranes were isolated by repeated Dounce homogenization in hypotonic (10 mM HEPES pH 7.5, 20 mM KCl, 10 mM $MgCl_2$, 50 µg/ml Pefabloc SC (Roth), 1 µg/ml Pepstatin A (Roth)) and hypertonic buffer (10 mM HEPES pH 7.5, 20 mM KCl, 10 mM $MgCl_2$, 1.0 M NaCl, 50 µg/ml Pefabloc SC, 1 µg/ml Pepstatin A). Purified membranes were resuspended in 30 ml hypotonic buffer supplemented with 10 µM ePTH, frozen in liquid nitrogen and stored at −80 °C until further use.

Frozen membranes were thawed on ice, and ePTH was added to 20 µM and incubated for 30 min. 2 mg/ml iodoacetamide (Sigma Aldrich) was added to the solution, which was then incubated for 30 min, Subsequently, the receptor was solubilized in 30 mM HEPES, pH 7.5, 500 mM NaCl, 10 mM KCl, 5 mM $MgCl_2$, 50 µg/ml Pefabloc SC, 1 µg/ml Pepstatin A, 1% (w/v) *n*-dodecyl-*β*-D-maltopyranoside (DDM, Anatrace) and 0.2% (w/v) cholesteryl hemisuccinate (CHS, Sigma Aldrich) at 4 °C for 2.5 h. Insoluble material was removed by ultracentrifugation, and the supernatant was incubated with TALON resin (GE Healthcare) at 4 °C, overnight.

The receptor-bound TALON resin was washed with 33 column volumes (CV) of Wash Buffer I (50 mM HEPES, pH 7.5, 500 mM NaCl, 10 mM $MgCl_2$, 5 mM imidazole, 10% (v/v) glycerol, 1.0% (w/v) DDM, 0.2% (w/v) CHS, 8 mM ATP, 5 µM ePTH), then 33 CV of Wash Buffer II (50 mM HEPES, pH 7.5, 500 mM NaCl, 15 mM imidazole, 10% (v/v) glycerol, 0.05% (w/v) DDM, 0.01% (w/v) CHS, 5 µM ePTH). The PTH1R–ePTH complex was eluted stepwise with four CV of Elution Buffer (50 mM HEPES, pH 7.5, 500 mM NaCl, 250 mM imidazole, 10% (v/v) glycerol, 0.05% (w/v) DDM, 0.01% (w/v) CHS, 20 µM ePTH). Protein-containing fractions were concentrated to 0.5 ml using a Vivaspin 2 concentrator (100 kDa molecular weight cutoff, Sartorius) and added to a PD MiniTrap G-25 column (GE Healthcare) equilibrated with G25 Buffer (50 mM HEPES pH 7.5, 500 mM NaCl, 10% (v/v) glycerol, 0.03% (w/v) DDM, 0.006% (w/v) CHS, 20 µM ePTH) to remove imidazole. The complex was treated for 6 h with His-tagged 3C protease and PNGaseF (both prepared in-house) to remove the N-terminal affinity tags and deglycosylate the receptor. After incubation with Ni-NTA resin overnight, cleaved receptor was collected as the flow-through and then concentrated to ~50 mg/ml using a Vivaspin 2 concentrator (100 kDa molecular weight cut-off). Protein concentrations were determined by absorbance at 280 nm on a Nanodrop 2000 spectrophotometer (Thermo Fisher Scientific). Protein purity and monodispersity were assessed by SDS–PAGE and analytical size-exclusion chromatography (Supplementary Fig. 3b,c).

Crystallization in lipidic cubic phase. The PTH1R–ePTH complex was crystallized using the in meso method at 20 °C. Concentrated receptor was mixed with molten lipid (90% (w/w) 9.9 MAG (Sigma Aldrich), 10% (w/w) cholesterol (Sigma Aldrich) at a ratio of 2:3 (v/v) using the twin-syringe method[50]. 40 nl boli were dispensed on 96-well glass bases (Swissci), overlaid with 800 nl precipitant solution using a Gryphon LCP crystallization robot (Art Robbins Instruments) and sealed with a coverglass. Optimized crystals used for data collection were grown in a precipitant condition consisting of 100 mM sodium citrate pH 6.0, 31% (v/v) PEG400, 300 mM sodium acetate and 20 µM ePTH. Single crystals were mounted with MiTeGen Dual-Thickness MicroMounts for data collection and cryo-cooled in liquid nitrogen without the addition of further cryoprotectant.

Data collection, structure determination and refinement. X-ray diffraction data were measured on an EIGER 16 M detector at the X06SA beamline at the Swiss Light Source (SLS) of the Paul Scherrer Institute (PSI) using a beam size of 10 × 10 µm. Datasets of PTH1R complexed with ePTH were collected using a beam attenuated to 25%, 0.1° of oscillation and 0.05 s exposure time. Data from 12 individual crystals were integrated using XDS[51]. Data merging and scaling was carried out using the program AIMLESS from the CCP4 suite[52,53]. Data collection statistics are reported in Table 1.

The structure of the PTH1R–ePTH complex was solved by molecular replacement (MR) with the program Phaser[54], using the transmembrane domain of the truncated human glucagon receptor (PDB 5EE7) with the fusion protein T4 lysozyme removed, the ECD of PTH1R (PDB 3C4M) and *Pyrococcus abyssi* glycogen synthase[55] (PDB 2BFW) as search models looking for one copy each. Manual model building was performed in COOT[56] using sigma-A weighted $2m|F_o|-|DF_c|$, $m|F_o|-D|F_c|$ maps using Buster (Global Phasing) and Phenix[57]. Initial refinement was carried out with REFMAC5 (ref. [58]) using maximum-likelihood restrained refinement in combination with the jelly-body protocol. Further and final stages of refinement were performed with Buster and Phenix.refine[59], with positional, individual isotropic *B*-factor and *TLS* refinement. The final refinement statistics are presented in Table 1.

Whole-cell ligand binding assay. HEK293T/17 cells (ATCC) were cultivated in Dulbecco's modified medium (Sigma) supplemented with 100 units/ml penicillin, 100 µg/ml streptomycin (Sigma) and 10 % (v/v) foetal calf serum (BioConcept). Cells were maintained at 37 °C in a humidified atmosphere of 5 % CO_2, 95% air. Transient transfections were performed with TransIT-293 (Mirus Bio) according to the manufacturer's instructions.

Ligand competition binding experiments were performed on whole HEK293T cells for comparison of affinities for wild-type and receptor mutants using a modified HTRF assay[60]. Receptor mutants were generated by site-directed mutagenesis and cloned into an expression vector containing an N-terminal SNAP-tag[61] (Cisbio). HEK293T cells were transiently transfected with receptor constructs and were seeded at 40,000 cells per well in poly-L-lysine-coated 384-well plates (Greiner). 48 h after transfection, cells were labeled with 50 nM SNAP-Lumi4-Tb (Cisbio) in assay buffer (20 mM HEPES pH 7.5, 100 mM NaCl, 3 mM $MgCl_2$ and 0.2% (w/v) non-fat milk) for 1.5 h at 37 °C. Cells were washed four times with assay buffer and were then incubated for 4 h at 4 °C in assay buffer containing 30 nM fluorescently labeled tracer peptide PTH-HL$_{647}$ (human [Nle$_{8,18}$, Y$_{34}$, C$_{35}$]PTH(1–34) labeled with HiLyte Fluor 647 at C$_{35}$ (Anaspec)) [60] and a concentration range of unlabelled wt PTH(1–34) (Bachem) as competitor. Fluorescence intensities were measured on an Infinite M1000 fluorescence plate reader (Tecan) with an excitation wavelength of 340 nm and emission wavelengths of 620 nm and 665 nm for Tb^{3+} and the fluorophore HiLyte Fluor 647, respectively. The ratio of FRET-donor and FRET-acceptor fluorescence intensities ($F_{665\,nm}/F_{620\,nm}$) was calculated. Total binding was defined by 30 nM PTH-HL$_{647}$ alone, and nonspecific binding was determined in the presence of 10 µM human wt PTH(1–34). Data were normalized to the specific binding for each individual experiment. To obtain IC$_{50}$ values, data were analyzed by global fitting to a one-site heterologous competition equation with the GraphPad Prism software (version 6.07, GraphPad).

Signaling assays. Ligand-induced cAMP and IP$_1$ (a metabolite of IP$_3$) accumulation was measured in transiently transfected HEK293T cells. 24 h after transfection, cells were washed with PBS, detached and resuspended in assay buffer (10 mM HEPES, pH 7.4, 1 mM $CaCl_2$, 0.5 mM $MgCl_2$, 4.2 mM KCl, 146 mM NaCl, 5.5 mM glucose, 0.1% (w/v) BSA). For cAMP accumulation measurements, cells were seeded at 5,000 cells per well in white 384-well plates (Greiner) and incubated for 30 min at 25 °C with a concentration range of human wt PTH(1–34) (Bachem) diluted in assay buffer supplemented with 1 mM 3-isobutyl-1-methylxanthin. cAMP accumulation was measured using the HTRF cAMP Dynamic2 kit (Cisbio) according to the manufacturer's protocol. For IP$_1$ measurements, cells were seeded at 20,000 cells per well in white 384-well plates (Greiner) and incubated for 2 h at

37 °C with a concentration range of human wt PTH(1-34) (Bachem) diluted in assay buffer supplemented with 50 mM LiCl. IP_1 accumulation was measured using the HTRF IP-One kit (Cisbio) according to the manufacturer's protocol. Data were normalised to the response of wt PTH1R at maximal ligand concentration and were analysed by a non-linear curve fit in GraphPad Prism.

Reporting Summary. Further information on research design is available in the Nature Research Reporting Summary linked to this article.

Data availability

Coordinates and structure factors have been deposited in Protein Data Bank (PDB 6FJ3). All other data are available from the corresponding authors upon reasonable request.

References

43. Schütz, M. et al. Directed evolution of G protein-coupled receptors in yeast for higher functional production in eukaryotic expression hosts. *Sci. Rep.* **6**, 21508 (2016).
44. Shimizu, N., Dean, T., Khatri, A. & Gardella, T. J. Amino-terminal parathyroid hormone fragment analogs containing alpha,alpha-di-alkyl amino acids at positions 1 and 3. *J. Bone Miner. Res.* **19**, 2078–2086 (2004).
45. Alexandrov, A. I., Mileni, M., Chien, E. Y. T., Hanson, M. A. & Stevens, R. C. Microscale fluorescent thermal stability assay for membrane proteins. *Structure* **16**, 351–359 (2008).
46. Klenk, C., Schulz, S., Calebiro, D. & Lohse, M. J. Agonist-regulated cleavage of the extracellular domain of parathyroid hormone receptor type 1. *J. Biol. Chem.* **285**, 8665–8674 (2010).
47. Yin, J., Mobarec, J. C., Kolb, P. & Rosenbaum, D. M. Crystal structure of the human OX2 orexin receptor bound to the insomnia drug suvorexant. *Nature* **519**, 247–250 (2015).
48. Rosenblatt, M., Goltzman, D., Keutmann, H. T., Tregear, G. W. & Potts, J. T. Chemical and biological properties of synthetic, sulfur-free analogues of parathyroid hormone. *J. Biol. Chem.* **251**, 159–164 (1976).
49. Neugebauer, W., Barbier, J. R., Sung, W. L., Whitfield, J. F. & Willick, G. E. Solution structure and adenylyl cyclase stimulating activities of C-terminal truncated human parathyroid hormone analogues. *Biochemistry* **34**, 8835–8842 (1995).
50. Caffrey, M. & Cherezov, V. Crystallizing membrane proteins using lipidic mesophases. *Nat. Protoc.* **4**, 706–731 (2009).
51. Kabsch, W. Integration, scaling, space-group assignment and post-refinement. *Acta Crystallogr. D Biol. Crystallogr.* **66**, 133–144 (2010).
52. Collaborative Computational Project, Number 4. The CCP4 suite: programs for protein crystallography. *Acta Crystallogr. D Biol. Crystallogr.* **50**, 760–763 (1994).
53. Evans, P. R. & Murshudov, G. N. How good are my data and what is the resolution? *Acta Crystallogr. D Biol. Crystallogr.* **69**, 1204–1214 (2013).
54. McCoy, A. J. et al. Phaser crystallographic software. *J. Appl. Crystallogr.* **40**, 658–674 (2007).
55. Horcajada, C., Guinovart, J. J., Fita, I. & Ferrer, J. C. Crystal structure of an archaeal glycogen synthase: insights into oligomerization and substrate binding of eukaryotic glycogen synthases. *J. Biol. Chem.* **281**, 2923–2931 (2006).
56. Emsley, P., Lohkamp, B., Scott, W. G. & Cowtan, K. Features and development of Coot. *Acta Crystallogr. D Biol. Crystallogr.* **66**, 486–501 (2010).
57. Adams, P. D. et al. PHENIX: a comprehensive Python-based system for macromolecular structure solution. *Acta Crystallogr. D Biol. Crystallogr.* **66**, 213–221 (2010).
58. Murshudov, G. N. et al. REFMAC5 for the refinement of macromolec ular crystal structures. *Acta Crystallogr. D Biol. Crystallogr.* **67**, 355–367 (2011).
59. Afonine, P. V. et al. Towards automated crystallographic structure refinement with phenix.refine. *Acta Crystallogr. D Biol. Crystallogr.* **68**, 352–367 (2012).
60. Emami-Nemini, A. et al. Time-resolved fluorescence ligand binding for G protein-coupled receptors. *Nat. Protoc.* **8**, 1307–1320 (2013).
61. Keppler, A. et al. A general method for the covalent labeling of fusion proteins with small molecules in vivo. *Nat. Biotechnol.* **21**, 86–89 (2003).

nature research

Corresponding author(s): Andreas Plückthun, PhD
Christoph Klenk, MD PhD

Reporting Summary

Nature Research wishes to improve the reproducibility of the work that we publish. This form provides structure for consistency and transparency in reporting. For further information on Nature Research policies, see Authors & Referees and the Editorial Policy Checklist.

Statistical parameters

When statistical analyses are reported, confirm that the following items are present in the relevant location (e.g. figure legend, table legend, main text, or Methods section).

n/a	Confirmed	
☒	☐	The exact sample size (*n*) for each experimental group/condition, given as a discrete number and unit of measurement
☐	☒	An indication of whether measurements were taken from distinct samples or whether the same sample was measured repeatedly
☐	☒	The statistical test(s) used AND whether they are one- or two-sided *Only common tests should be described solely by name; describe more complex techniques in the Methods section.*
☒	☐	A description of all covariates tested
☒	☐	A description of any assumptions or corrections, such as tests of normality and adjustment for multiple comparisons
☒	☐	A full description of the statistics including central tendency (e.g. means) or other basic estimates (e.g. regression coefficient) AND variation (e.g. standard deviation) or associated estimates of uncertainty (e.g. confidence intervals)
☒	☐	For null hypothesis testing, the test statistic (e.g. *F*, *t*, *r*) with confidence intervals, effect sizes, degrees of freedom and *P* value noted *Give P values as exact values whenever suitable.*
☒	☐	For Bayesian analysis, information on the choice of priors and Markov chain Monte Carlo settings
☒	☐	For hierarchical and complex designs, identification of the appropriate level for tests and full reporting of outcomes
☒	☐	Estimates of effect sizes (e.g. Cohen's *d*, Pearson's *r*), indicating how they were calculated
☐	☒	Clearly defined error bars *State explicitly what error bars represent (e.g. SD, SE, CI)*

Our web collection on statistics for biologists may be useful.

Software and code

Policy information about availability of computer code

Data collection	All software used in structure determination is mentioned in the text.
Data analysis	All software used in data analysis is mentioned in the text.

For manuscripts utilizing custom algorithms or software that are central to the research but not yet described in published literature, software must be made available to editors/reviewers upon request. We strongly encourage code deposition in a community repository (e.g. GitHub). See the Nature Research guidelines for submitting code & software for further information.

Data

Policy information about availability of data

All manuscripts must include a data availability statement. This statement should provide the following information, where applicable:

- Accession codes, unique identifiers, or web links for publicly available datasets
- A list of figures that have associated raw data
- A description of any restrictions on data availability

Coordinates and structure factors have been deposited in the Protein Data Bank (PDB ID: 6FJ3).

Field-specific reporting

Please select the best fit for your research. If you are not sure, read the appropriate sections before making your selection.

☒ Life sciences ☐ Behavioural & social sciences ☐ Ecological, evolutionary & environmental sciences

For a reference copy of the document with all sections, see nature.com/authors/policies/ReportingSummary-flat.pdf

Life sciences study design

All studies must disclose on these points even when the disclosure is negative.

Sample size	n/a, the study reports a crystal structure and biochemical assays, which have been done in the number of replicates indicated in the text.
Data exclusions	No data were excluded.
Replication	The biochemical assays were carried out in the number of replicates indicated in the text.
Randomization	n/a
Blinding	n/a

Reporting for specific materials, systems and methods

Materials & experimental systems

n/a	Involved in the study
☒	☐ Unique biological materials
☒	☐ Antibodies
☐	☒ Eukaryotic cell lines
☒	☐ Palaeontology
☒	☐ Animals and other organisms
☒	☐ Human research participants

Methods

n/a	Involved in the study
☒	☐ ChIP-seq
☒	☐ Flow cytometry
☒	☐ MRI-based neuroimaging

Eukaryotic cell lines

Policy information about cell lines

Cell line source(s)	Only HEK293T/17 cells were used, obtained from ATCC.
Authentication	No authentication was used, as the experiments depend only on transient transfection of a recombinant protein.
Mycoplasma contamination	Since the cells were freshly obtained from ATCC, no mycoplasma testing was used.
Commonly misidentified lines (See ICLAC register)	n/a